Experimental Implementation of an All-Optical Interferometric Drop, Add, and Extract Multiplexer for Superchannels

Simon J. Fabbri, Stylianos Sygletos, Andreas Perentos, Erwan Pincemin, Kate Sugden, and Andrew D. Ellis

(Invited Paper)

***Abstract*—We present the experimental implementation of an all-optical ROADM scheme for routing of an individual subchannel within an all-optical OFDM superchannel. The different functions required of optical node were demonstrated using interferometric technique with the extraction, drop, and addition of individual subchannel in a ten subchannels optically aggregated signal. The scheme we reported enables a fully flexible node compatible with future terabit per second superchannel transmission.**

***Index Terms*—All-optical node, all-optical OFDM, flexible optical networks, interferometer, optical communication, subcarrier multiplexing.**

I. Introduction

As the load on the optical networks steadily grows, an optimum utilization of the legacy optical fibre infrastructure is essential. Only flexible superchannel based optical networks can make use of the entire transmission window available [1]. While many research groups are approaching the fundamental limit of standard fibre point-to-point systems [2], optical networks require the use of reconfigurable optical add/drop multiplexers (ROADM) [3]. The convergence of flexible superchannel capable of carrying terabit per second of data with flexible optical nodes is paramount to extend the benefit of optical link capacity to optical networks. Future optical networks will require the high granularity necessary to aggregate and extract data from an optical link with a range going from the single channel to multi-terabit wide superchannel.

Different channel types have the potential to form superchannels for these future networks with small spectral guard band such as OFDM [4] and Nyquist WDM [5], [6] or even with overlapping spectra such as time-frequency packing [7] or all-optical OFDM (AO-OFDM) [8]–[12]. High performance optical filters such as those used in [4] allow for a diminution of the guardband while maintaining a high quality signal. However, the guardband remains finite. Recently, solutions compatible with overlapping spectrum have been presented conceptually [13], [14] with a preliminary demonstration using four wave mixing (FWM) [15]. The extract function of the node, which consists in removing a particular channel from a superchannel to free the spectrum allocated, can be obtained using an interferometric solution. It offers the advantage of dropping the channel of interest from the superchannel without impacting the adjacent channels. When reaching the optical node, the superchannel is divided in two paths, the through arm and the channel extraction arm. While one path is unaltered, the channel to be dropped is demultiplexed from the superchannel and reshaped. The reshaped signal is then interferometrically combined with the original superchannel, and the relative phase is adjusted for destructive interference. This approach offers the possibility to implement ROADMs with guardband free and overlapping spectrum. Recent proof of concept has been implemented emulating an interferometer composed of an electrical and optical path [15]. However, the scheme proposed is quite complex since it requires the use of a coherent receiver and a high-speed transmitter as part of the node. Moreover, the interferometric structure was associated with a complex FWM process to insert new data in the superchannel.

Recently, our group has proposed the design [16] and the experimental implementation [17] of a new architecture, which we call terabit interferometric drop, add and extract (TIDE) multiplexer, to facilitate all-optical switching of sub-channels within the OFDM signal band, see Fig. 1. Switching is performed in two layers. In the upper layer, the super-channel selection takes place using typical Wavelength Selective Switch (WSS)

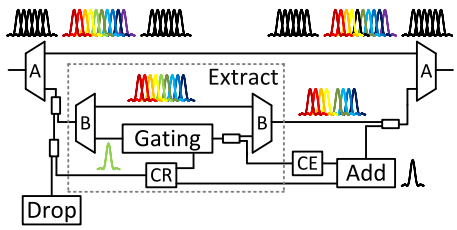

Fig. 1. All-Optical TIDE node. Optical filter A: coarse WSS for superchannel selection, optical filter B: fine WSS for channel selection. CR: clock recovery. CE: carrier extraction.

Manuscript received October 6, 2014; revised December 18, 2014; accepted December 22, 2014. Date of publication January 8, 2015; date of current version March 4, 2015. The work was supported by the EU-ICT Project FOX-C, under Grant "318415" and by the Marie Currie-IEF Project ARTISTE, under Grant "330697."

S. J. Fabbri is with the Physics Department, University College Cork, Cork, Ireland, and also with the Aston Institute of Photonic Technologies, Aston University, Birmingham B4 7ET, U.K. (e-mail: s.fabbri@aston.ac.uk).

S. Sygletos, A. Perentos, K. Sugden, and A. D. Ellis are with the Aston Institute of Photonic Technologies, Aston University, Birmingham B4 7ET, U.K. (e-mail: s.sygletos@aston.ac.uk; a.perentos@aston.ac.uk; k.sugden@aston.ac.uk; andrew.ellis@aston.ac.uk).

E. Pincemin is with Orange Labs Networks, 08005 Lannion, France (e-mail: erwan.pincemin@orange.com).

Color versions of one or more of the figures in this paper are available online at http://ieeexplore.ieee.org.

Digital Object Identifier 10.1109/JLT.2015.2390292

units. Sub-channel switching is performed at a lower layer, with an interferometric setup that allows coherent subtraction of the dropped signals and the addition of the new. Contrary to the previous approaches, our scheme makes use of purely *all-optical* methods, such as FFT/i-FFT filtering and time domain sampling, to replicate the waveform of any sub-channel for the extract operation. Clock recovery, carrier extraction and phase locking units will be also needed for data and frequency synchronization within the node to implement an in-line operation in a transmission link.

In this paper, we extend on our previously reported work [17] on the TIDE architecture by showing for the first time transparency to single (BPSK) and dual (QPSK) quadrature signals. In both cases we note the use of an AO-OFDM signal with fully overlapped spectra. The paper is structured such as Section II describes the AO-OFDM transmitter and the implementation of the all-optical node, Section III, provides a detailed description of the experimental results for the BPSK operation, and in Section IV, our recent extension to accommodate operation with QPSK signals is given, along with the corresponding performance evaluation results.

II. Experimental Implementation of the TIDE Node

The experimental setup is shown in Fig. 2. The schematic represents the AO-OFDM transmitter and the two parts of the node corresponding to the extract functions (blue box) and to the add function (yellow box).

A. AO-OFDM Transmitter

A fibre laser with a kilohertz class linewidth was positioned at a wavelength of approximately 1552.7 nm. The optical carrier was then modulated using a pulse pattern generator generating a 10 Gb/s 2^{15}–1 bits long pattern, a broadband electrical amplifier and a high bandwidth optical Mach–Zehnder modulator (MZM). The resultant 10 Gb/s BPSK channel, shown in Fig. 2(a), was used in conjunction with a second MZM, driven at approximatively 2 V_π by a 20 GHz sine wave and biased to generate a 20 GHz spaced five line comb, to obtain five BPSK channels. In order to maintain strict frequency spacing between channels, the same 10 GHz RF master clock source was used through the system. An additional five channels, frequency shifted by 10 GHz were generated using a parallel path structure. The first arm of this structure contained an optical frequency shifter, using a dual-parallel MZM driven by the electrical signal frequency provided by the system clock source. The unshifted frequency and negatively shifted components after the frequency conversion were suppressed by more than 30 dB with respect to the frequency shifted channels [18]. The second arm contained an attenuator, a polarization controller, an optical delay line, and a phase shifter. The two arms were recombined, interleaving the two sets of five channels to form the ten line AO-OFDM transmitter. The two arms were mismatched by a strict integer number of bit periods (the fiber length equivalent of 5 bit periods), polarization aligned and power equalized. An additional polarization beam splitter was positioned at the output of the AO-OFDM transmitter in order to guarantee polarization alignment of the odd and even subchannels. In this experiment, ten BPSK 10 Gb/s channels formed the 100 Gb/s single polarization AO-OFDM superchannel, shown in Fig. 2(b).

Unless either guard bands [19] or ideal filters and pulse shapes [20] are used AO-OFDM transmitters typically benefit from a phase stabilization circuit [21] to contain the residual crosstalk. This is shown as stabilization circuit 1 in Fig. 2 and was employed to maximize the back to back performance when BPSK signal were used. The principle used here is the conversion of the relative phase of adjacent subcarriers into an amplitude variation through the use of FWM with an arbitrary laser pump such that the amplitude variation may be directly detected using a low frequency photodiode [22]. A small number of AO-OFDM channels were filtered before being combined with a pump signal positioned at 320 GHz from the AO-OFDM laser source before being amplified up to 0.5 W. The signal and pump were inserted into a 400 m HNLF spool, of nonlinear coefficient γ: $\sim$7 $W^{-1}\cdot km^{-1}$. One of the FWM products generated by the interaction between two adjacent sub-channels and the pump is dependent on the relative phase variation between the sub-channels. Because of the symmetrical FWM process a narrow sinc-shaped fibre Bragg grating (FBG) filter [23] was positioned at 320 GHz on the other side of the superchannel before being detected by a low speed photodiode. The optical power variation at the photodiode was approximately of 13 dB between an in-phase adjacent subcarriers and $\pi/2$ phase difference. A computer controlled low speed ADC/DAC was used to implement the stabilization loop by piloting the high tension voltage applied to a piezoelectric ceramic (PZT) stretcher [24] with optical fibre looped around it which acted as the phase shifter in one arm of the parallel path structure. We note that this scheme could also be used to recover a low jitter RF clock for distribution throughout the TIDE node [25].

In addition to the subcarrier relative phase control, the time delay between the data source and the comb generation system had a significant impact on the performance with a difference of nearly 5 dB in the Q^2-factor measured between the best and the worst relative data delay. As it has been extensively explained in [21], the time alignment directly impacts the level of residual crosstalk when non ideal filters are employed.

The coherent receiver employed an independent fibre laser forming a tunable local oscillator which was tuned to within 100 MHz of the sub-channel to be measured. The AO-OFDM signal was sampled at the receiver at approximately 8 samples per bit. Channel selection was performed using a digitally implemented sinc-function matched filter. Channel estimation was achieved off-line using typical digital signal processing algorithms for clock recovery, polarization rotation, and frequency offset compensation [26], [27].

B. All Optical TIDE Node

The all-optical node comprised two distinct structures: a combined drop/extract interferometer and an add interferometer. The interferometric suppression of the channel to be removed from the superchannel allows for the channel clear function even for the strongly overlapped AO-OFDM modulation format without additional guardband.

The interferometric suppression of a channel requires the extraction of a copy of the superchannel before its recombination

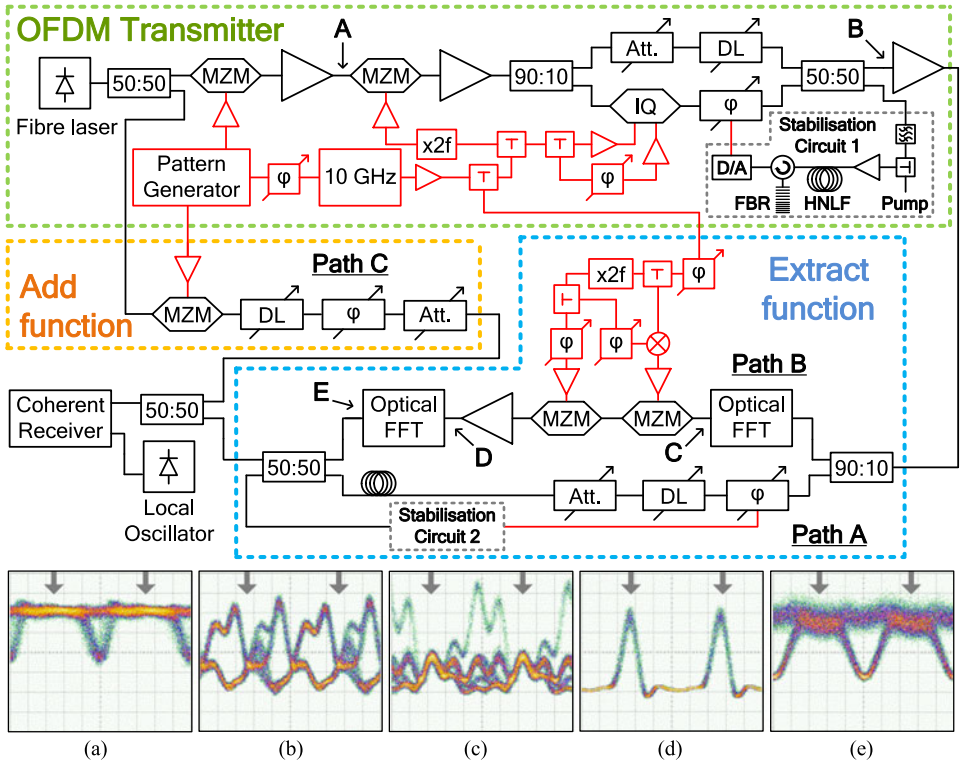

Fig. 2. Top: Experimental setup of the AO-OFDM transmitter (top, green frame) and of the proposed all optical ROADM with drop and extract function (bottom, blue frame, path A & B) and emulation of the add function (middle, orange frame, path C). Polarisation controllers and monitoring couplers not pictured for clarity. Black and red lines signify optical and electrical paths respectively. MZM: Mach–Zehnder modulator, DL: tunable delay line, φ: tunable phase shifter, Att.: tunable attenuator, IQ: dual parallel MZM, HNLF: highly nonlinear fibre, FBG: fibre Bragg grating, D/A: digital/analog converter, triangles represent optical or electrical amplifiers. Bottom: Intensity eye diagrams at various points: (a) individual channel before superchannel multiplexing, (b) BPSK AO-OFDM superchannel, (c) demultiplexed channel after optical channel selection through optical FFT filter, (d) sampled channel after optical gating, and (e) reshaped channel prior to interferometric extract operation. Arrows represent the center of the eye. Time window equals to two bit period, 30 GHz electrical bandwidth.

with the original AO-OFDM signal. The channel to be dropped is extracted by an optical FFT based AO-OFDM demultiplexer [19], [28], [29] and sampled using an optical gate. The resultant optical samples are then reshaped to resemble a single channel using a second optical FFT. The two paths are combined with appropriate phase, power, and polarization alignment such that the channel to be dropped is interferometrically suppressed and thus implementing the function of extracting or clearing a sub-channel from the original superchannel. The add-drop operation is completed by adding a signal with the correct channel frequency.

In the experimental implementation presented here, the first optical FFT, enabling the target channel to be dropped, was implemented as an optical second order FFT. It consisted of two delay line interferometers (DLI) with free spectral ranges (FSR) of 20 and 40 GHz, respectively, followed by a 0.4 nm filter with an approximately Gaussian shape. Since this filter can only approximate the ideal optical FFT (fourth order in this case), there was residual crosstalk, the impact of which was minimized using the phase control within the AO-OFDM transmitter. The dropped channel prior to optical gating (see Fig. 2(c)) shows a clear cross-talk free point.

In order to extract this channel from the AO-OFDM superchannel, the dropped channel needs to be reshaped, so that it may be interferometrically subtracted from the AO-OFDM signal. Since low crosstalk is only obtained at the optimum sampling instant (indicated by arrows in Fig. 2(a)–(e)), an optical gate was used after the FFT based filter to remove the crosstalk at other possible sampling times. The level of this crosstalk is of course influenced by imperfect filtering in the TIDE node and finite transmitter bandwidth, both of which impact the adjacent channels orthogonality required in OFDM. The optical gate selects the time period corresponding to the dropped channel bit during each OFDM symbol. The gating window width was optimized using numerical simulation [16] where a tradeoff between short widths and long pulse widths exists. A narrow pulse train approaches the ideal Dirac comb which would sample only the bit pattern required at the ideal sampling instant and avoid residual crosstalk, whereas a larger pulse reduces the impact of sampling induced noise enhancement [30]. More intuitively, in order to maximize signal energy, the gate selects as much of the middle part of the eye diagram as possible whilst still suppressing the adjacent parts influenced by the residual crosstalk. The optical sampling in the node was obtained by driving two optical MZMs so it produces short pulse train [31]. The first MZM was driven by a strong 20 GHz RF signal and biased such as it produced a narrow pulse train. The second MZM suppressed every second pulse. To maximize this suppression, the drive signal for this MZM was obtained by modulating the 20 GHz signal by a 10 GHz RF signal using a broadband mixer and time aligning the

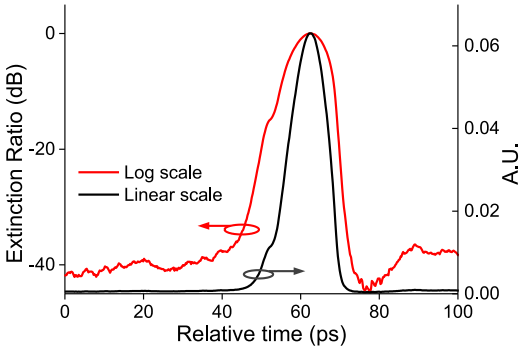

Fig. 3. Optical pulse obtained from the optical gating cascaded MZMs structure when time scanned using a picosecond wide pulse, FWHM = 11.6 ps, extinction ratio >35 dB. Logarithmic and linear scale in red and black, respectively.

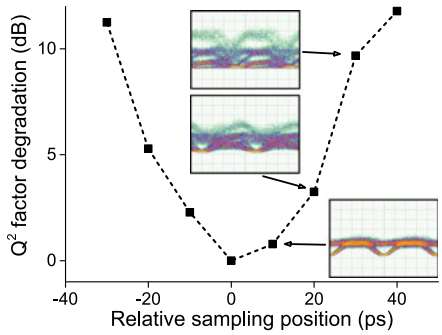

Fig. 4. Q^2-factor degradation for the reshaped AO-OFDM channel as function of the time position of the optical sampling within the bit period, eyediagrams (over two periods, 100 mV/div.) showing the reshaped BPSK channel for different sampling position.

resultant electrical pulse. The sampling window obtained has a FWHM of 11.6 ps and an extinction ratio greater than 35 dB (see Fig. 3). The sampled output shows in Fig. 2(d) where a phase modulated RZ signal is observed, free of any noticeable crosstalk.

After gating, a second optical FFT was used to reshape the channel to be dropped. This stage consisted of single 20 GHz FSR DLI followed by a WSS filter. The first stage FFT was required due to limited resolution of the used WSS, however recent reports suggest that a WSS based DFT capable of directly processing a 10 Gbaud AO-OFDM signal is possible [32]. Q^2-factor penalties induced by misaligned sampling timing with a selection of corresponding eye-diagrams of the resulting reshaping are shown in Fig. 4. In addition to showing the impact of the time alignment of the optical gating on the reshaping of the extracted channel (measured at point E in Fig. 2), the narrow operating range shown in the figure confirms the requirement for a narrow optical gating window to reduce the residual crosstalk and so obtain a clear RZ-BPSK signal. The timing misalignment results in a degradation of the channel suppression as the signal of the two arms interfering is different. The monitoring of the extract function coupled with a clock recovery module driving the gating function would lead to the system independence from the transmitter clock.

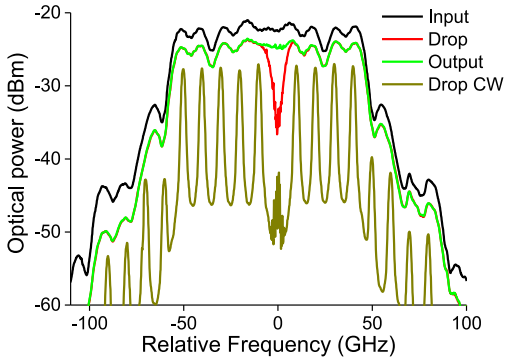

Fig. 5. Optical spectrum of the BPSK AO-OFDM signal at the input of the node (black), after one channel was extracted (red) and after the addition of a new channel at the output of the node (green), stabilization systems active.

The channel dropped, gated and reshaped was combined with the copy of the original AO-OFDM signal. Consequently, the channel of interest was suppressed from the superchannel when the two arms were path matched, polarization aligned, power matched, and out of phase, as illustrated in Fig. 5. However, our experimental node demonstration was based on optical fibre and discrete devices in a research laboratory environment, where the optimum interference condition may only be achieved for short period of time. A second stabilization circuit was implemented in order to mitigate the thermally and mechanically (fan) induced phase difference between the two arm of the 89.4 m long extract interferometer. A phase locked loop circuit (stabilization circuit 2 in Fig. 2) was implemented by controlling the phase relation between the interferometer arms using a second PZT fibre stretcher. The power at the output of the drop interferometer was monitored with a low speed photodiode to control when the signal of both arm are out of phase. In order to follow the power variation at the wavelength of the dropped channel a narrow filter (bandwidth less than the signal bandwidth) was placed before the photodiode. In addition to the filter and to increase the sensitivity of the stabilization circuit, a 27 kHz dithering tone was added to the superchannel. The optical signal carrying the small variation was down converted using the photodiode before being amplified and mixed with the original dithering signal. The lock-in amplifier circuitry followed by appropriate electrical filtering allows for high sensitivity and consequently good stabilization performance [33]. Digital processing was used to close the loop and control the phase difference between the interferometer arms through a fiber stretcher. While channel rejection higher than 20 dB may be observed for short period of time, the few hundred hertz bandwidth feedback circuitry stabilized the drop function operation, with a reasonable channel rejection in the range of 10–15 dB. Fig. 5 illustrates the comb line suppression as the channel suppression representation is limited by the optical spectrum analyser 2 GHz resolution convolved with the signal bandwidth (10 GHz). Note that since different filters were used for each function in this demonstration, with an electrical filter shaping the transmitter pulses and an optical FFT filter the pulse shape within the node, a small mismatch in the pulse shapes was observed which in consequence slightly degraded the quality of the interference pattern.

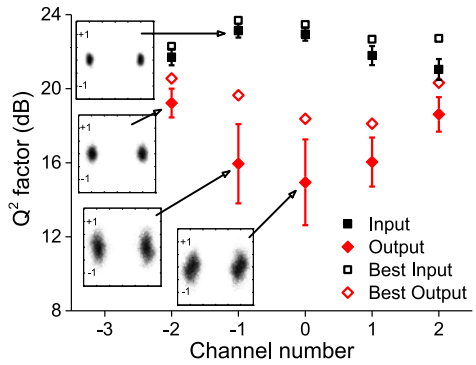

Fig. 6. Q^2-factor measurement for the five central channels BPSK modulated: Input (square) and output after extraction and addition (diamond). Channel zero carrying new data after extract function. 160k sample per acquisition, statistics over 40 continuous acquisitions.

The add function was implemented by adding a third arm to the optical interferometer. As previously, this arm had to be carefully aligned to the two other arms both in power, polarization, and time. The time delay was set to be an exact integer number of bit and the polarization alignment was controlled using a polarization beam splitter at the output of the node. The new channel to be combined to the OFDM superchannel was generated using the second port of the pattern generator through a different data modulator to the OFDM transmitter. However, the optical carrier originated from the same laser so the added channel was well aligned to the freed spectrum after the drop function. Optical carrier extraction has been previously demonstrated and could be readily implemented in order to obtain a system with solely an external optical reference [34]. The output of the TIDE node was consequently a single polarization AO-OFDM superchannel carrying a new set of information on one of its subcarrier. Since this implementation had polarization sensitive devices (MZIs, gate), a single polarization superchannel was manipulated. To eliminate polarization sensitivity, integration or a free-space interferometer could be used alongside a polarization insensitive optical gate [35]. In addition, the all-optical nature of the concept requires the optical dispersion and dispersion mode dispersion compensation.

Since the matched filter in the coherent receiver closely approximated the ideal pulse shape the residual crosstalk was low, and no phase control was required for the add channel.

III. TIDE All-Optical Node With BPSK AO-OFDM

Performance measurements were taken at the coherent receiver for the AO-OFDM signal before and after the optical node. Fig. 6 presents the Q^2-factor measured for the five central channels, the channel labeled no. 0 being the one where the drop and add function occurred. The Q^2-factor, in decibel, was calculated from the error vector magnitude following the expression $Q^2 = 10\log_{10}(1/\mathrm{EVM}^2)$ [36]. The error bars represent one standard deviation obtained from 40 measurements of 160k samples and illustrate the fluctuations in Q^2-factor due to residual drop interferometer variations. In addition, the mean Q^2-factor (solid symbols) and the best Q^2-factor (open symbols) from these sets of measurement are presented to show the potential of such scheme if it was integrated and/or fully-stabilized. When a new channel was added in place of the vacant spectrum, penalties where observed due to the imperfect channel drop. Q^2-factor degradations are believed to be due to: (i) a residual mismatch between the pulse shape of the original and reshaped signals, (ii) mean phase errors due to phase dithering to stabilize the TIDE node and (iii) excess amplified spontaneous emission due to noise sampling and the insertion loss of the FFT's and the optical gate [16]. Due to a sharp trade-off experienced during WSS profile optimization between under-filtering, resulting in sharp transitions but residual sidebands from the optical gating, and over-filtering, resulting into slower bit transition and poor interferometric suppression, we believe that pulse shape matching dominated the performance. Comparing the subplot A and E in Fig. 2 is a good illustration of the limitation of this first experimental implementation. The degradation of the reshaped channel can be observed from the broadening of the transition period in the bit period, along with the residual crosstalk due to the imperfect demultiplexing filter. The use of higher FFT order, appropriate transmitter pulse shaping and/or a more versatile WSS should therefore reduce the observed penalty significantly. The Fig. 6 insets display the BPSK constellation diagrams for Q^2-factor values for individual measurements close to the average value for each channel. The figure clearly shows good performance at the output of the TIDE node. As expected, the penalty was greatest for the wavelength at which channel had been extracted and added, even if it is interesting to note its remained with considerable margin above the typical 7%-overhead Hard Decision FEC threshold.

IV. TIDE All-Optical Node With QPSK AO-OFDM

Whilst the positive result presented in the previous section is encouraging, little net benefit is derived from overlapping carriers at the symbol rate if only one quadrature is used for modulation. While it is clear that the TIDE node will be compatible with broader superchannels, it is critical that the concept is compatible with more spectrally efficient modulation formats employing both quadratures. Here we verify compatibility with QPSK formatted superchannels.

A small number of minor modifications were applied to the experimental implementation of the node. In order to minimize the amount of ASE noise generated from the amplifier situated in the reshaping arm of the interferometer, all monitor taps were removed before the gating function. In addition, an improved optical FFT was used for both channel selection and reshaping. The channel selection was obtained using a cascade of tunable DLI of FSR 20 and 42.8 GHz, respectively, and a WDM interleaver of FSR 50 GHz was used to select a single channel. Although a slight frequency misalignment was unavoidable in the second (athermal) DLI used, the overall transfer function of the optical filter offers a large improvement in the channel selection particularly for the suppression of the channel located at ± 40 GHz from the channel selected. The reshaping function was obtained by cascading two DLIs, of FSR 20 and 40 GHz, along with a sharp optical filter to remove the additional frequency components remaining from the incomplete FFT function.

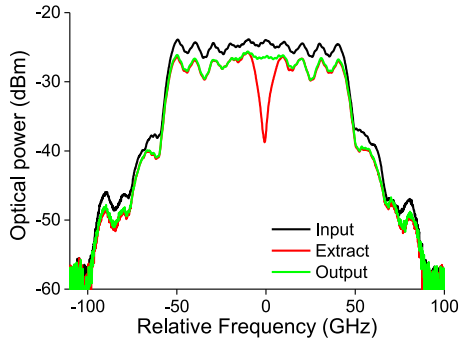

Fig. 7. Optical spectrum of the QPSK AO-OFDM signal at the input of the node (black), after one channel was extracted (red) and after the addition of a new channel at the output of the node (green), stabilization systems active.

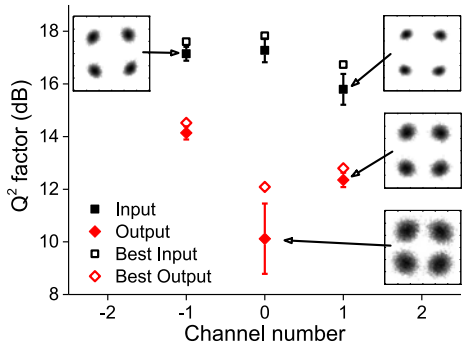

Fig. 8. Q^2-factor measurement for the five central channels QPSK modulated: Input (square) and output after extraction and addition (diamond). Channel zero carrying new data after extract function. 160k sample per acquisition, statistics over 40 continuous acquisitions.

The transmitter phase stabilization circuitry was modified to account for dual quadrature modulation (QPSK is modulation stripped on the fourth harmonic) and used to maintain the phase relation between adjacent subcarriers at the transmitter. As observed for BPSK, the matched filter in the coherent receiver tolerates different phase relationship between subcarriers and phase control is not required. However, the channel selection in the optical domain was imperfect and thus the control of the relative phase was observed to improve the performance at the output of the optical node. The stabilization system delivered more than 1.3 dB Q^2-factor margin due to the crosstalk confinement away from the decision point, in this case sampled by the optical gating, and thus the imperfect demultiplexing penalty was mitigated.

Finally, the TIDE node was completed by adding new data to the channel cleared by the extract section. For QPSK data, the same optical modulator was used for the original superchannel and for the channel added, with the add channel data decorrelated from the superchannel by the path length delay. Fig. 7 displays the optical spectrum for the input superchannel, the channel drop and the resulting superchannel with the new channel added. With the assistance of the second stabilization circuit, the channel suppression was maintained higher than 10 dB as the dither based feedback loop, based on the suppression of the channel power, is not affected by the modulation format. For each data point, the coherent receiver recorded 40 sets of 160k samples which were processed offline. When receiving a single QPSK channel, the average Q^2-factor measured from the EVM was 21.5 dB. The laser, used both at the transmitter and at the receiver had a narrow tunable range only allowing the measurement of the central channel where the drop and add occurred and the adjacent channels. Fig. 8 presents the measurement of the superchannel at the input of the optical node and at its output when the central channel had been suppressed and new data had been added. Identically to the Fig. 6, the main degradation is observed on the central channel. Nevertheless the performance is maintained above FEC limits. Adjacent channels were somewhat affected but to a lesser extent due to the improved channel reshaping implemented for the quadrature modulation format. The standard deviation of the Q^2-factor results for those channels was also reduced, demonstrating a regime closer to the optimum orthogonality and hence the independence of one channel to the other.

In order to scale the bit rate, improved filters would be required for higher order modulation and for increased subchannel counts. Consequently, a modest reduction in the optical switching window width would be required. In addition to the increase in capacity, those modifications, coupled with an improved stabilization circuitry, would lead also the way to cascadability of the TIDE node.

V. Conclusion

In this paper, we present the implementation of a TIDE node for AO-OFDM superchannels with overlapping carriers. The standard node functions, channel drop, extraction, and insertion, were obtained whilst the signals remained fully in the optical domain. A channel was extracted through optical FFT filtering, reshaped using optical gating and a second optical FFT filter and then interferometrically erased from the AO-OFDM superchannel in a fully optical structure, allowing the insertion of a new set of data. The scheme demonstrated here operates for both single and dual quadrature formats, and clearly scales to multi-terabit/s superchannels through the use of additional sub-channels, and opens the way for guardband-free all-optical flexible transport.

References

[1] T. J. Xia, S. Gringeri, and M. Tomizawa, "High-capacity optical transport networks," *IEEE Commun. Mag.*, vol. 50, no. 11, pp. 170–178, Nov. 2012

[2] X. Liu, S. Chandrasekhar, and P. J. Winzer, "Digital signal processing techniques enabling multi-Tb/s superchannel transmission: An overview of recent advances in DSP-enabled superchannels," *IEEE Signal Process. Mag.*, vol. 31, no. 2, pp. 16–24, Mar. 2014.

[3] A. Sano, H. Masuda, E. Yoshida, T. Kobayashi, E. Yamada, Y. Miyamoto, F. Inuzuka, Y. Hibino, Y. Takatori, K. Hagimoto, T. Yamada, and Y. Sakamaki, "30 × 100-Gb/s all-optical OFDM transmission over 1300 km SMF with 10 ROADM nodes," presented at the Eur. Conf. Opt. Commun., Berlin, Germany, 2007, Paper PD.1.7.

[4] E. Pincemin, M. Song, J. Karaki, A. Poudoullec, N. Nicolas, M. Van der Keur, Y. Jaouen, P. Gravey, M. Morvan, and G. Froc, "Multiband OFDM transmission with sub-band optical switching," presented at the Eur. Conf. Opt. Commun., London, U.K., 2013, Paper Th.2.A.1.

[5] G. Bosco, V. Curri, A. Carena, P. Poggiolini, and F. Forghieri, "On the performance of Nyquist-WDM terabit superchannels based on PM-BPSK, PM-QPSK, PM-8QAM or PM-16QAM subcarriers," *J. Lightw. Technol.*, vol. 29, no. 1, pp. 53–61, Jan. 2011.

[6] E. Palkopoulou, G. Bosco, A. Carena, D. Klonidis, P. Poggiolini, and I. Tomkos, "Nyquist-WDM-based flexible optical networks: Exploring physical layer design parameters," *J. Lightw. Technol.*, vol. 31, no. 14, pp. 2332–2339, Jul. 2013.

[7] L. Poti, G. Meloni, G. Berrettini, F. Fresi, M. Secondini, T. Foggi, G. Colavolpe, E. Forestieri, A. D'Errico, F. Cavaliere, R. Sabella, and G. Prati, "Casting 1 Tb/s DP-QPSK communication into 200 GHz bandwidth," presented at the Eur. Conf. Exhib. Opt. Commun., Amsterdam, The Netherlands, 2012, Paper P4.19.

[8] A. D. Ellis and F. C. G. Gunning, "Spectral density enhancement using coherent WDM," *Photon. Technol. Lett.*, vol. 15, no. 2, pp. 504–506, 2005.

[9] W. Shieh and C. Athaudage, "Coherent optical orthogonal frequency division multiplexing," *Electron. Lett.*, vol. 42, no. 10, pp. 587–589, 2006.

[10] A. Sano, E. Yamada, H. Masuda, E. Yamazaki, T. Kobayashi, E. Yoshida, Y. Miyamoto, R. Kudo, K. Ishihara, and Y. Takatori, "No-guard-interval coherent optical OFDM for 100 Gb/s long-haul WDM transmission," *J. Lightw. Technol.*, vol. 27, no. 16, pp. 3705–3713, Aug. 2009.

[11] G. Goldfarb, G. Li, and M. G. Taylor, "Orthogonal wavelength division multiplexing using coherent detection," *Photon. Technol. Lett.*, vol. 19, no. 24, pp. 2015–2017, 2007.

[12] Y. Chen, J. Li, C. Zhao, L. Zhu, F. Zhang, Y. He, and Z. Chen, "Experimental demonstration of ROADM functionality on an optical SCFDM superchannel," *Photon. Technol. Lett.*, vol. 24, no. 3. pp. 215–217, 2012.

[13] M. G. Taylor, "Coherent optical channel substitution," U.S. Patent 8 050 564, Nov. 1, 2011.

[14] P. J. Winzer, "An opto-electronic interferometer and its use in subcarrier add/drop multiplexing," *J. Lightw. Technol.*, vol. 31, no. 11, pp. 1775–1782, Jun. 2013.

[15] T. Richter, C. Schmidt-Langhorst, R. Elschner, T. Kato, T. Tanimura, S. Watanabe, and C. Schubert, "Coherent in-line substitution of OFDM subcarriers using fiber-frequency conversion and free-running lasers," presented at the Opt. Fiber Commun. Conf. Exhib., San Francisco, CA, USA, 2014, Paper Th.5.B.6.

[16] S. Sygletos, S. J. Fabbri, E. Giacoumidis, M. Sorokina, D. Maron, M. F. C. Stephens, D. Klonidis, I. Tomkos, and A. D. Ellis, "A novel architecture for all-optical add-drop multiplexing of OFDM signals," presented at the Eur. Conf. Opt. Commun., Cannes, France, 2014, Paper We.1.5.4.

[17] S. J. Fabbri, S. Sygletos, E. Pincemin, K. Sugden, and A. D. Ellis, "First experimental demonstration of terabit interferometric drop, add and extract multiplexer," presented at the Eur. Conf. Opt. Commun., Cannes, France, 2014, Paper We.1.5.2.

[18] S. J. Fabbri, C. O'Riordan, S. Sygletos, and A. D. Ellis, "Active stabilisation of single drive dual-parallel Mach–Zehnder modulator for single sideband signal generation," *Electron. Lett.*, vol. 49, no. 2, pp. 135–136, 2013.

[19] D. Hillerkuss, M. Winter, M. Teschke, A. Marculescu, J. Li, G. Sigurdsson, K. Worms, S. Ben Ezra, N. Narkiss, W. Freude, and J. Leuthold, "Simple all-optical FFT scheme enabling Tbit/s real-time signal processing," *Opt. Exp.*, vol. 18, no. 9, pp. 9324–9340, 2010.

[20] J. Zhao and A. Ellis, "Electronic impairment mitigation in optically multiplexed multicarrier systems," *J. Lightw. Technol.*, vol. 29, no. 3, pp. 278–290, Feb. 2011.

[21] S. K. Ibrahim, J. Zhao, F. G. Gunning, P. Frascella, F. H. Peters, and A. D. Ellis, "Towards a practical implementation of coherent WDM: Analytical, numerical, and experimental studies," *IEEE Photon. J.*, vol. 2, no. 5, pp. 833–847, Oct. 2010.

[22] P. Frascella, S. Sygletos, and A. D. Ellis, "A novel phase stabilization scheme for DPSK CoWDM signals using high order four wave Mmixing," presented at the Eur. Conf. Opt. Commun., Geneva, Switzerland, 2011, Paper We.8.A.2.

[23] I. Bennion, J. A. R. Williams, L. Zhang, K. Sugden, and N. J. Doran, "Uv-written in-fibre Bragg gratings," *Opt. Quantum Electron.*, vol. 28, pp. 93–135, 1996.

[24] D. A. Jackson, R. Priest, A Dandridge, and A. B. Tveten, "Elimination of drift in a single-mode optical fiber interferometer using a piezoelectrically stretched coiled fiber," *Appl. Opt.*, vol. 19, no. 17, pp. 2926–9, 1980.

[25] M. J. Power, W. Jia, R. P. Webb, R. J. Manning, and F. C. G. Gunning, "Four-wave mixing for clock recovery of phase modulated optical OFDM superchannel," *Opt. Exp.*, vol. 22, no. 6, p. 7007, 2014.

[26] S. J. Savory, "Digital coherent optical receivers: Algorithms and subsystems," *J. Sel. Topics Quantum Electron.*, vol. 16, no. 5, pp. 1164–1179, 2010.

[27] E. Pincemin, N. Brochier, M. Selmi, O. Z. Chahabi, P. Ciblat, and Y. Jaouen, "Novel blind equalizer for coherent DP-BPSK transmission systems: Theory and experiment," *IEEE Photon. Technol. Lett.*, vol. 25, no. 18, pp. 1835–1838, Sep. 2013.

[28] A. J. Lowery, "Design of arrayed-waveguide grating routers for use as an optical OFDM demultiplexers," *Opt. Exp.*, vol. 18, no. 13, pp. 14129–14143, 2010.

[29] K. Lee, C. T. D. Thai, and J. K. Rhee, "All-optical discrete Fourier transform processor for 100 Gbps OFDM transmission," *Opt. Exp.*, vol. 16, no. 6, pp. 4023–4028, 2008.

[30] A. Naka, T. Matsuda, and S. Saito, "Receiver performance analysis and basic design for optical time division multiplexed transmission systems," *Electron. Commun. Jpn., Part 1, Commun.*, vol. 83, no. 4, pp. 93–104, 2000.

[31] A. D. Ellis, T. Widdowson, X. Shan, and D. G. Moodie, "Three-node, 40 Gbit/s OTDM network experiment using eletro-optic switches," *Electron. Lett.*, vol. 30, no. 16, pp. 1333–1334, 1994.

[32] R. Rudnick, A. Tolmachev, D. Sinefeld, O. Golani, S. Ben-Ezra, M. Nazarathy, and D. M. Marom, "Sub-banded/single-sub-carrier drop-demux and flexible spectral shaping with a fine resolution photonic processor," presented at the Eur. Conf. Opt. Commun., Cannes, France, 2014, Paper PD.4.1.

[33] S. J. Fabbri, S. Sygletos, and A. D. Ellis, "Multi-harmonic optical comb generation," presented at the 38th Eur. Conf. Exhib. Opt. Commun., Amsterdam, The Netherlands, 2012, Paper Mo.2.A.2.

[34] S. K. Ibrahim, S. Sygletos, R. Weerasuriya, and A. D. Ellis, "Novel real-time homodyne coherent receiver using a feed-forward based carrier extraction scheme for phase modulated signals," *Opt. Exp.*, vol. 19, no. 9, pp. 8320–8326, 2011.

[35] D. D. Marcenac, A. D. Ellis, and D. G. Moodie, "80 Gbit/s OTDM using electro-absorption modulators," *Electron. Lett.*, vol. 34, no. 1, pp. 101–103, 1998.

[36] R. Schmogrow, B. Nebendahl, M. Winter, A. Josten, D. Hillerkuss, S. Koenig, J. Meyer, M. Dreschmann, M. Hueber, C. Koos, J. Becker, W. Freude, and J. Leuthold, "Error vector magnitude as a performance measure for advanced modulation formats," *Photon. Technol. Lett.*, vol. 24, no. 1, pp. 61–63, 2012.

Authors' biographies not available at the time of publication.